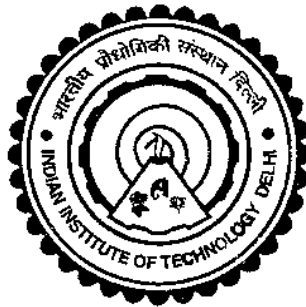


EXPERIMENTAL AND NUMERICAL (TWO- AND
THREE-DIMENSIONAL) INVESTIGATION OF PARTICLE
TRAPPING PERFORMANCE OF SEDIMENT INVERT
TRAPS (SIT) FITTED IN RECTANGULAR OPEN
CHANNEL

SALMAN BEG



DEPARTMENT OF CIVIL ENGINEERING
INDIAN INSTITUTE OF TECHNOLOGY DELHI
MARCH, 2025

© Indian Institute of Technology Delhi (IITD), New Delhi, 2025

EXPERIMENTAL AND NUMERICAL (TWO- AND
THREE-DIMENSIONAL) INVESTIGATION OF PARTICLE
TRAPPING PERFORMANCE OF SEDIMENT INVERT
TRAPS (SIT) FITTED IN RECTANGULAR OPEN
CHANNEL

by

SALMAN BEG

Department of Civil Engineering

Submitted

in fulfilment of the requirements of the degree of Doctor of Philosophy
to the



INDIAN INSTITUTE OF TECHNOLOGY DELHI
MARCH, 2025

CERTIFICATE

This is to certify that the thesis entitled “**Experimental and Numerical (Two- and Three-Dimensional) Investigation of Particle Trapping Performance of Sediment Invert Traps (SIT) Fitted in Rectangular Open Channel**”, being submitted by **Mr. Salman Beg** to the Indian Institute of Technology Delhi, New Delhi, India for the award of the degree of **Doctor of Philosophy** in Civil Engineering, is a bonafide research work carried out by him under my supervision and guidance. The thesis, in my opinion, has reached the standard of fulfilling the requirement for the award of Doctor of Philosophy degree. The research report and the results presented in this thesis have not been submitted in parts or in full to any other University or Institute for the award of any degree or diploma.

March, 2025

Dr. Deo Raj Kaushal
(Supervisor)
Professor
Department of Civil Engineering
Indian Institute of Technology Delhi
New Delhi-110016

Acknowledgments

I bow in reverence to the Almighty God whose benign benediction gave me the required zeal for completion of this work.

I wish to express my sincere gratitude to my revered and learned supervisor Dr. Deo Raj Kaushal, Professor, Department of Civil Engineering, Indian Institute of Technology Delhi, New Delhi, India for his illuminating, scholarly guidance and creative supervision right from its inception to its culmination in the present work. He has always been inexhaustible source of inspiration and guidance to me. Without his unceasing encouragement and cooperation this work would not have completed. I humbly acknowledge a lifetime's gratitude to him.

I would like to express my gratitude to Prof. Vasant Matsagar, Head, Department of Civil Engineering, former HOD's (Prof. Manoj Dutta, Prof. N. K. Garg, Prof. G. V. Ramana and Prof. A. K. Nema), internal members of SRC (Prof. R. R. Kalaga, Prof. S. Chakma, Department of Civil Engineering) and external member of SRC (Prof. S. S. Sinha, Department of Applied Mechanics) for their co-operative attitude, valuable comments and suggestions throughout the study period.

I owe a deep sense of gratitude to the All-pervading Spirit whose divine light provided me the perseverance, guidance, inspiration, faith and strength to carry on even when the going got tough. My special sincere, heartfelt gratitude and indebtedness are due to my Paternal Aunt, Uncle and Father, for their sincere prayers, constant encouragement and blessings.

I wish to express my deep sense of gratitude to late Prof. M. Jamil, Civil Engineering Department, AMU, Aligarh for his encouraging, caring words, inspiration and guidance which have contributed in a significant way towards

completion of this thesis. I do not have words to express his all kindness and help. I pray for him, for the best returns from Almighty.

I am deeply thankful to Dr. M. Mohsin, Associate Professor, University Polytechnique, AMU, Aligarh for sharing his knowledge in performing PIV experiments.

I am deeply grateful for the moral and uplifting support extended to me by my esteemed colleagues, Dr. Himanshu Pratap Singh, Dr. Sandhya Gupta, Dr. Aravind Kumar Bairwa, Miss Stuti Mishra, Mr. Harshwardhan, Mr. Yatindra Kumar, Mr. Gaurav and all other members of the Simulation Lab who have been instrumental in my journey.

I would also like to extend my thanks to Mr. Nena Ram Gehlot, Mr. Yaad Ram and Mr. Sharan who consistently demonstrated their willingness to provide assistance in the Simulation Laboratory of Water Resource Engineering section. I would like to express my sincere gratitude to the esteemed members of the Civil Engineering Department, particularly Mr. Rajveer Agrawal and Mr. Randheer, for their invaluable assistance with various official matters. Their contributions have been instrumental in the successful completion of this scholarly pursuit. Anyone who assisted me in any way with my research, whether it was directly or indirectly, deserves my deepest gratitude.

March, 2025

Salman Beg

Abstract

Sewer systems in cities are an important part of the subterranean infrastructure that will be important for a long time to come. Due to increased urbanization, major construction projects generate enormous volumes of construction debris and dust, having sediment particles which settles on building rooftops, parking lots, highways and streets. Stormwater sewer inlets, open drains, and gully pots carry sediments and heavy metals from impermeable surfaces like roadways, parking lots and building roofs into combined sewers after rainfall and high winds. Smaller sediment particles move as a suspended load in combined sewers, stormwater sewers, or open drains, whereas bigger particles roll, slide, and saltate. In summer, when sewers and open stormwater drainage channels have low water flow, sediment builds up on the channel bed. Excessive sedimentation reduces the cross-section of open stormwater drainages and sewer conduits, reducing their flow capacity and causing sewer water to spill out, causing flooding or waterlogging and environmental nuisance. Stormwater runoff and sewer water which is often silty, reduce the efficiency of sewage treatment plant pumps and hydropower dam turbines. Pollutants sticking on sediment may harm aquatic life and water quality of receiving water bodies.

The sedimentation problem in stormwater sewer channels and drainages has led to the development and use of sedimentation mitigation devices. In-line combined sewage detention tanks (CSDT) and grit chambers placed strategically along stormwater channel reaches reduce silt and optimize channel performance. Unfortunately, grit chambers and in-line CSDTs retain organic material with sediment particles, which stinks, and sediment particles escape at high velocity. Slotted sediment invert traps (SITs) reduce particle settling in sewers and stormwater drains without the downsides of grit chambers and detention tanks, according to previous

research. A sediment invert trap (SIT) is a bucket (closed on all sides except top) below the channel bottom that traps sediments that fall in. For assessing the particle trapping performance of SIT, a number of design aspects of SIT such as the shape of SIT, slot sizes, flow depth, sediment size and tilt of SIT have been studied earlier by investigators, experimentally and computationally. In experimental studies, previous investigators have used actual and artificial particles; in two- and three-dimensional computational analysis, spherical particles have been considered in the discrete phase model (DPM) of ANSYS Fluent. However, natural sediments (or sewer sediments) have a non-spherical shape. Earlier investigators have tested SITs of single horizontal and vertical dimensions; however, variation in depth, length and width of SITs can affect its particle trapping efficiency. Moreover, for two-dimensional (2D) and three-dimensional (3D) computational modeling, previous researchers assumed the lid geometry to be a thin line and a plane, respectively. A certain thickness of upstream and downstream lids was proven to exist above the top of the SIT, as shown by the geometry of the actual SIT demonstrated by Schmitt *et al.* (1999). In earlier studies, rectangular and trapezoidal SITs of single depth have been extensively studied through simulation-based modeling using a fixed lid modeling approach in which an open channel flume was considered a conduit closed from all sides and flow in it was under pressure. In fact, the flow in open channels is under gravity and has a distinct free water surface exposed to the atmosphere.

There is a scope for a study on the design aspects of SITs, such as the shape and depth of SIT, lid-thickness of SIT, actual shape of sediment particle and development of empirical particle trap efficiency predictors for predicting the particle trapping performance of rectangular, irregular hexagonal and trapezoidal SITs. An experimental as well as computational investigation is needed to study the effect of

the shape and depth of the SIT, the lid-thickness of SIT, and the actual shape of sediment particles on the particle trap efficiency of the SIT.

This study was started firstly with measurements of velocity distribution in an open channel and SITs using 2D particle image velocimetry (PIV) experimental set-up to visualize the velocity vector field and predict sewer sediment settlement, erosion, and deposition patterns inside slotted rectangular, irregular hexagonal, and trapezoidal sewer SITs. Secondly, a three-dimensional simulation-based case study examined the importance of including lid-thickness (t) and particle shape factor (ϕ) in simulation modeling for prediction of particle trap efficiency of SIT. After that, a separate extensive experimental study examined how the shape and depth of SIT, lid-thickness of SIT, actual shape of sediment particle affects the particle trap efficiency of rectangular, irregular hexagonal and trapezoidal SITs at three depths of flow, with five sewer sediment size ranges, and two slot aperture sizes. For experiments, real sewer sediments collected from the stormwater sewers was used with laboratory-scaled 5 m long and 0.15 m wide open channel flume with bottom-fitted slotted SITs. Under the same conditions and parameters of experimental study, a two- and three-dimensional computational study was carried out to propose an improved simulation modeling to bring an improvement in the prediction of particle trap efficiency of rectangular, irregular hexagonal and trapezoidal SITs by incorporating the thickness of lids in the simulation model geometry and the particle shape factor of real sewer sediment particles into the discrete phase model (DPM). The present 2D and 3D predictions of particle trap efficiency of each SIT was carried out using both spherical and non-spherical drag laws in DPM. The present simulation studies used ANSYS Fluent 2020 R1 CFD software, including the volume of fluid (VOF) model, $k-\epsilon$ (realizable type) turbulence model, and DPM. In the end, multiple nonlinear regression analysis was done utilizing Microsoft Excel's generalized reduced gradient

(GRG) solver to develop the empirical trap efficiency predictors for rectangular, irregular hexagonal, and trapezoidal SITs.

The flow velocities at the central vertical plane of open channel flume obtained through PIV measurements were in satisfactory agreement with those predicted by 3D-CFD simulations and equation of Yang *et al.* (2004). Similarly, average flow velocities in open channel flume measured by the EMF were in satisfactory agreement with those predicted by 3D-CFD simulations and equation of Yang *et al.* (2004). At all flow depths in open channel flume, the magnitude of velocities measured by the PIV in the SITs was consistently lower than those predicted by 3D-CFD simulations, in all depth and shape of SITs. The case study showed that lid-thickness and particle shape factor significantly affected the particle trap efficiency of SIT. However, the effect of the particle shape factor was found more dominant than that of the lid-thickness. Experimental and 2D & 3D simulated particle trap efficiency of rectangular, irregular hexagonal, and trapezoidal SITs increased with depth of SIT, but the trend was not uniform for a specific range of sewer sediment sizes, slot aperture sizes, and flow depths. In 2D and 3D simulation modeling, using the experimental data of the present study, the consideration of the lid-thickness (t) in the geometry of the lids and shape factor (ϕ) of real non-spherical sewer sediment particles in the DPM model brought 2D and 3D predicted particle trap efficiency closer to experimental findings as compared to the 2D and 3D predictions with spherical particles, which indicates that the proposed simulation modeling is successfully validated and can be used by hydraulic engineers as a replacement of experiments to design the SITs for sewer solid management. Additionally, regardless of spherical and non-spherical drag laws and lid-thickness, it was found in 2D and 3D simulations that variations in turbulent kinetic energy (TKE) in the slot aperture region with variations in the depth of SIT, depth of flow, and slot aperture size

affected the particle trap efficiency of each SIT. Three-dimensional (3D) simulation modeling outperformed 2D simulation modeling, with predicted particle trap efficiency values closer to experimental values. In general, 3D predicted particle trap efficiencies are lower than 2D predicted particle trap efficiencies which is due to the reason that in case of 3D simulations, the TKE in the slot aperture region was higher than in the case of 2D simulations. The 3D predicted average velocity and velocity vector field in an open channel flume and SITs had been satisfactorily validated with PIV observations. Hence, it is verified that the selected VOF and realizable $k-\epsilon$ turbulence models of ANSYS Fluent CFD software are robust for studying the flow through open channel flumes with SITs attached below their bottom bed. The free water surface and water hump formation above the SITs, as tracked by the VOF model, was nearly identical to what was seen experimentally, indicating successful validation of the numerical simulations and robustness of the VOF model. The fixed lid model is not capable to simulate such realistic water surface profiles. Empirical regression models developed for predicting particle trap efficiency of rectangular, irregular hexagonal, and trapezoidal SITs performed well in terms of R , R^2 , and $MAPE$.

This study concluded that out of the selected three SIT geometries, the overall best shape of the SIT is rectangular, which yielded maximum particle trap efficiency both experimentally and computationally by trapping the more fraction of sediment particles in a given sewer sediment size range. Out of the two slot aperture sizes of 0.15 m and 0.03 m, use of slot aperture size of 0.15 m in the entire range of depth of SIT (y) covered in the present study provides maximum particle trap efficiency which can be used by hydraulic design engineers for implementing on the existing or new storm water sewers and urban open channel drainages. Based on the careful analysis of the variation of particle trap efficiency with varied depth of rectangular SIT, sewer

sediment size range, flow depth and slot aperture size, it is suggested to use depth of rectangular SIT (y) in the range of $0.38 \text{ m} \leq y \leq 0.65 \text{ m}$ with slot aperture size of 0.15 m and depth of rectangular SIT equal to 0.38 m with slot aperture size of 0.03 m . The best suitable simulation models for modeling the fluid flow in an open channel with bottom-fitted SITs is the VOF and $k-\epsilon$ turbulence models.

सार (सारांश)

शहरों में सीवर प्रणालियाँ भूमिगत बुनियादी ढांचे का एक महत्वपूर्ण हिस्सा हैं जो आने वाले लंबे समय तक महत्वपूर्ण रहेंगी। बढ़ते शहरीकरण के कारण, प्रमुख निर्माण परियोजनाएं भारी मात्रा में निर्माण मलबा और धूल उत्पन्न करती हैं, जिसमें तलछट के कण होते हैं जो इमारतों की छतों, पार्किंग स्थलों और राजमार्गों और सड़कों पर जमा हो जाते हैं। बारिश और तेज़ हवाएँ तलछट और भारी धातुओं को अभेद्य सतहों जैसे सड़कों, पार्किंग स्थलों और इमारत की छतों से स्टार्मवाटर सीवर इनलेट, खुली नालियाँ और गल्ली पोट के रास्ते से संयुक्त सीवर में ले जाते हैं। छोटे तलछट कण संयुक्त सीवरों, स्टार्मवाटर सीवरों या खुली नालियों में सस्पेंडिड लोड के रूप में चलते हैं, जबकि बड़े कण लुढ़कते, फिसलते और उछलते हुए चलते हैं। गर्मियों में जब सीवर और खुले स्टार्मवाटर ड्रेनेज चैनलों में पानी का प्रवाह कम होता है, तो चैनल के तल पर तलछट जमा हो जाती है। अत्यधिक तलछट जमाव खुले स्टार्मवाटर ड्रेनेज और सीवर नाली के क्रॉस-सेक्शन को कम कर देता है, जिससे उनकी प्रवाह क्षमता कम हो जाती है और सीवर का पानी बाहर फैल जाता है, जिससे बाढ़ या जलभराव और पर्यावरणीय परेशानी होती है। स्टार्मवाटर अपवाह और सीवर पानी जो अक्सर गादयुक्त होता है, सीवेज उपचार संयंत्र पंपों और जलविद्युत बांध टर्बाइनों की दक्षता को कम कर देता है। तलछट पर चिपके प्रदूषक जलीय जीवन और जल निकायों की जल गुणवत्ता को नुकसान पहुंचा सकते हैं।

स्टार्मवाटर सीवर चैनलों और जल निकासी में अवसादन की समस्या के कारण अवसादन शमन उपकरणों का विकास और उपयोग हुआ है। इन-लाइन संयुक्त सीवेज डिटेंशन टैंक (सीएसडीटी) और ग्रिट चैंबर रणनीतिक रूप से स्टार्मवाटर चैनल के साथ लगाए जाते हैं, जो गाद को कम करते हैं और चैनल के प्रदर्शन को अनुकूलित करते हैं। दुर्भाग्य से, ग्रिट चैंबर और इन-लाइन सीएसडीटी कार्बनिक पदार्थों को तलछट कणों के साथ बनाए रखते हैं, जिससे बदबू आती है और तलछट के कण उच्च वेग से निकल जाते हैं। पिछले शोध के अनुसार, स्लॉटेड सेडिमेंट इनवर्ट ट्रेप्स (एसआईटी) में वो खामियाँ नहीं होतीं जो ग्रिट चैंबर और डिटेंशन टैंक में होती हैं और एसआईटी बहुत कुशलता से सीवर और स्टार्मवाटर नालियों में कणों के जमाव को कम करते हैं। सेडिमेंट इनवर्ट ट्रेप (एसआईटी) चैनल के तल के नीचे एक बाल्टी (ऊपर को छोड़कर सभी तरफ से बंद) होती है जो अंदर गिरने वाले तलछट को फंसाती है। एसआईटी के

कण फंसाने के प्रदर्शन का आकलन करने के लिए, एसआईटी के कई डिजाइन पहलुओं जैसे कि एसआईटी का आकार, स्लॉट का आकार, प्रवाह की गहराई, तलछट का आकार और एसआईटी के झुकाव का अध्ययन जांचकर्ताओं द्वारा पहले प्रयोगात्मक और कम्प्यूटेशनल रूप से किया गया है। प्रायोगिक अध्ययनों में, पिछले जांचकर्ताओं ने वास्तविक और कृत्रिम कणों का उपयोग किया है; दो- और तीन-आयामी कम्प्यूटेशनल विश्लेषण में, ANSYS फ्लुएंट के डिसकिरीट फेज़ मॉडल (डीपीएम) में कणों को गोलाकार माना गया है। हालाँकि, प्राकृतिक तलछट (या सीवर तलछट) का आकार गैर-गोलाकार होता है। पहले जांचकर्ताओं ने एकल क्षैतिज और ऊर्ध्वाधर आयामों के एसआईटी का परीक्षण किया है; हालाँकि, एसआईटी की गहराई, लंबाई और चौड़ाई में भिन्नता इसकी कण ट्रेप दक्षता को प्रभावित कर सकती है। इसके अलावा, दो-आयामी (२डी) और तीन-आयामी (३डी) कम्प्यूटेशनल मॉडलिंग के लिए, पिछले शोधकर्ताओं ने लिड्स ज्यामिति को क्रमशः एक पतली रेखा और एक पतली शीट माना था। अपस्ट्रीम और डाउनस्ट्रीम लिड्स की एक निश्चित मोटाई एसआईटी के शीर्ष के ऊपर मौजूद साबित हुई थी, जैसा कि श्मिट *एट अल.* (१९९९) द्वारा प्रदर्शित वास्तविक एसआईटी की ज्यामिति द्वारा दिखाया गया था। पहले के अध्ययनों में, एकल गहराई के आयताकार और ट्रेपेज़ॉइडल एसआईटी का फिकस्ड लिड मॉडलिंग दृष्टिकोण का उपयोग करके सिमुलेशन-आधारित मॉडलिंग के माध्यम से बड़े पैमाने पर अध्ययन किया गया है, जिसमें एक खुले चैनल फ्लूम को सभी तरफ से बंद नाली माना जाता था और इसमें प्रवाह दबाव के अधीन था। वास्तव में, खुले चैनलों में प्रवाह गुरुत्वाकर्षण के अधीन होता है और इसमें वायुमंडल के संपर्क में आने वाली जल सतह होती है।

एसआईटी के डिजाइन पहलुओं पर अध्ययन की गुंजाइश है, जैसे एसआईटी का आकार और गहराई, एसआईटी के लिड्स की मोटाई, तलछट कण का वास्तविक आकार और आयताकार, अनियमित हेक्सागोनल और ट्रेपेज़ॉइडल एसआईटी के कण फंसाने के प्रदर्शन का आकलन करने के लिए अनुभवजन्य कण जाल दक्षता भविष्यवक्ताओं का डेवलपमेंट। एसआईटी के कण जाल दक्षता पर एसआईटी के आकार और गहराई, एसआईटी के लिड्स की मोटाई और तलछट कणों के वास्तविक आकार के प्रभाव का अध्ययन करने के लिए एक प्रयोगात्मक और साथ ही कम्प्यूटेशनल जांच की आवश्यकता है।

इस अध्ययन की शुरुआत सबसे पहले एक खुले चैनल और एसआईटी में वेग वितरण के माप के साथ की गई थी, जिसमें वेग वेक्टर क्षेत्र को देखने और स्लॉटेड आयताकार, अनियमित हेक्सागोनल और ट्रैपेज़ॉइडल सीवर एसआईटी के अंदर सीवर तलछट का गिरना, क्षरण और जमाव पैटर्न का पूर्वानुमान लगाने के लिये २डी पारटिकल इमेज विलासिमीटरी (पीआईवी) प्रयोगात्मक सेट-अप का उपयोग किया गया था। इसके बाद एक तीन-आयामी सिमुलेशन-आधारित केस अध्ययन से एसआईटी की कण जाल दक्षता के पूर्वानुमान के लिए सिमुलेशन मॉडलिंग में लिड्स की मोटाई (t) और कण आकार कारक (ϕ) को शामिल करने के महत्व की जांच की। उसके बाद, एक अलग व्यापक प्रयोगात्मक अध्ययन ने जांच की कि एसआईटी का आकार और गहराई, एसआईटी के लिड्स की मोटाई, तलछट कण का वास्तविक आकार किस तरह आयताकार, अनियमित हेक्सागोनल और ट्रैपेज़ॉइडल एसआईटी की कण जाल दक्षता को प्रभावित करता है, प्रवाह की तीन गहराई पर, पांच सीवर तलछट के आकार श्रेणियाँ और दो स्लॉट एपर्चर आकार के साथ। प्रयोगों के लिए, स्टार्मवाटर सीवरों से एकत्र किए गए वास्तविक सीवर तलछट का उपयोग प्रयोगशाला-स्केल के ५ मीटर लंबे और ०.१५ मीटर चौड़े खुले चैनल फ्लूम और बॉटम-फिटेड स्लॉटेड एसआईटी के साथ किया गया था। प्रायोगिक अध्ययन की समान शर्तों और मापदंडों के तहत, आयताकार, अनियमित हेक्सागोनल और ट्रैपेज़ॉइडल एसआईटी की कण जाल दक्षता की अनुमानिता में सुधार लाने के लिए और एक बेहतर सिमुलेशन मॉडलिंग का प्रस्ताव करने के लिए दो- और तीन-आयामी कम्प्यूटेशनल अध्ययन किया गया था जिसमें सिमुलेशन मॉडल ज्यामिति में लिड्स की मोटाई और डिसकिरीट फेज़ मॉडल (डीपीएम) में वास्तविक सीवर तलछट कणों के कण आकार कारक (ϕ) को शामिल किया गया। प्रत्येक एसआईटी की कण जाल दक्षता की वर्तमान २डी और ३डी भविष्यवाणियां डीपीएम में गोलाकार और गैर-गोलाकार ड्रैग कानूनों का उपयोग करके की गईं। वर्तमान सिमुलेशन अध्ययनों में ANSYS फ्लुएंट २०२० R१ सीएफडी सॉफ्टवेयर का उपयोग किया गया है, जिसमें वाल्यूम ओफ फ्लूइड (वीओएफ) मॉडल, $k-\epsilon$ (रियालाइज़िबिल) टरबुलेंस मॉडल और डीपीएम शामिल हैं। अंत में, आयताकार, अनियमित हेक्सागोनल और ट्रैपेज़ॉइडल एसआईटी के लिए अनुभवजन्य जाल दक्षता भविष्यवक्ताओं को विकसित करने के लिए माइक्रोसॉफ्ट एक्सेल के जेनरालाइज़्ड रिडयूज़्ड ग्रेडिएंट (जीआरजी) सॉल्वर का उपयोग करके मल्टीपल नॉनलाइनियर रिग्रेशन विश्लेषण किया गया था।

खुले चैनल फ्लूम के केंद्रीय ऊर्ध्वाधर तल पर पीआईवी माप के माध्यम से प्राप्त प्रवाह वेग ३डी-सीएफडी सिमुलेशन और यांग *एट अल.* (२००४) के समीकरण द्वारा पूर्वानुमानित वेगों के साथ संतोषजनक रूप से मेल खाते थे। इसी तरह, ओपन चैनल फ्लूम में इलेक्ट्रो मेगनेटिक फ्लो मीटर (ईएमएफ) द्वारा मापे गए औसत प्रवाह वेग ३डी-सीएफडी सिमुलेशन और यांग *एट अल.* (२००४) के समीकरण द्वारा पूर्वानुमानित वेगों के साथ संतोषजनक रूप से मेल खाते थे। खुले चैनल फ्लूम में सभी प्रवाह गहराइयों पर, एसआईटी की सभी गहराई और आकार में पीआईवी द्वारा मापे गए वेगों का परिमाण ३डी-सीएफडी सिमुलेशन द्वारा मापे गए परिमाण से कम था। तीन-आयामी सिमुलेशन-आधारित केस अध्ययन से पता चला कि लिड्स की मोटाई और कण आकार कारक ने एसआईटी की कण जाल दक्षता को महत्वपूर्ण रूप से प्रभावित किया। हालाँकि, कण आकार कारक का प्रभाव लिड्स की मोटाई की तुलना में अधिक प्रभावी पाया गया। आयताकार, अनियमित हेक्सागोनल और ट्रेपेज़ॉइडल एसआईटी की प्रायोगिक और २डी और ३डी सिमुलेटेड कण जाल दक्षता एसआईटी की गहराई के साथ बढ़ी, लेकिन बढ़ने की प्रवृत्ति सीवर तलछट आकार, स्लॉट एपर्चर आकार और प्रवाह गहराई की एक विशिष्ट श्रृंखला के लिए एक समान नहीं थी। २डी और ३डी सिमुलेशन मॉडलिंग में, वर्तमान अध्ययन के प्रयोगात्मक डेटा का उपयोग करते हुए, डीपीएम मॉडल में वास्तविक गैर-गोलाकार सीवर तलछट कणों के आकार कारक (ϕ) और लिड्स की ज्यामिति में लिड की मोटाई (t) पर विचार करके कण जाल दक्षता की भविष्यवाणी की गई। २डी और ३डी सिमुलेशन मॉडलिंग में गोलाकार कणों के साथ जाल दक्षता की भविष्यवाणियों की तुलना में वास्तविक गैर-गोलाकार कणों के साथ जाल दक्षता प्रायोगिक निष्कर्षों के करीब है जो इंगित करता है कि प्रस्तावित सिमुलेशन मॉडलिंग सफलतापूर्वक मान्य है जिसका उपयोग हाइड्रोलिक इंजीनियरों द्वारा प्रयोगों के प्रतिस्थापन के रूप में और सीवर प्रबंधन के लिए एसआईटी को डिजाइन करने के लिए किया जा सकता है। इसके अतिरिक्त, गोलाकार और गैर-गोलाकार ड्रैग कानूनों और लिड्स की मोटाई की परवाह किए बिना, २डी और ३डी सिमुलेशन में पाया गया कि स्लॉट एपर्चर क्षेत्र में टरबुलेंस काइनेटिक एनर्जी (टीकेई) में भिन्नता एसआईटी की गहराई, प्रवाह की गहराई और स्लॉट एपर्चर आकार में भिन्नता के साथ है जिसने प्रत्येक एसआईटी की कण जाल दक्षता को प्रभावित किया। ३डी सिमुलेशन मॉडलिंग ने २डी सिमुलेशन मॉडलिंग से बेहतर प्रदर्शन किया, जिसमें अनुमानित कण जाल दक्षता प्रयोगात्मक कण

जाल दक्षता के करीब थे। सामान्य तौर पर, ३डी पूर्वानुमानित कण जाल दक्षताएं २डी पूर्वानुमानित कण जाल दक्षताओं से कम हैं, जिसका कारण यह है कि ३डी सिमुलेशन के मामले में, स्लॉट एपर्चर क्षेत्र में टीकेई २डी सिमुलेशन के मामले की तुलना में अधिक था। एक खुले चैनल फ्लूम और तलछट इनवर्ट ट्रेप में ३डी सिमुलेशन से अनुमानित किया गया औसत वेग और वेग वेक्टर क्षेत्र पीआईवी अवलोकनों के साथ संतोषजनक ढंग से मान्य किया गया। इसलिए, यह सत्यापित है कि खुले चैनल फ्लूम्स और उनके निचले बेड के नीचे लगे एसआईटी के माध्यम से प्रवाह का अध्ययन करने के लिए ANSYS फ्लुएंट सीएफडी सॉफ्टवेयर के चयनित वीओएफ और रियालाइज़िबिल $k-\epsilon$ टर्बुलेंस मॉडल सबसे उपयुक्त हैं। एसआईटी के ऊपर पानी की सतह और पानी के उठाव का गठन, जैसा कि वीओएफ मॉडल द्वारा ट्रैक किया गया था, लगभग वैसा ही था जैसा प्रयोगात्मक रूप से देखा गया था, जो संख्यात्मक सिमुलेशन के सफल सत्यापन और वीओएफ मॉडल की मजबूती का संकेत देता है। फिकस्ड लिड मॉडल ऐसी यथार्थवादी जल सतह प्रोफाइल का अनुकरण करने में सक्षम नहीं है। आयताकार, अनियमित हेक्सागोनल और ट्रैपेज़ॉइडल एसआईटी की कण जाल दक्षता का पूर्वानुमान लगाने के लिये प्रस्तावित किये गये अनुभवजन्य प्रतिगमन मॉडल ने R , R^2 और $MAPE$ के संदर्भ में अच्छा प्रदर्शन किया।

इस प्रयोगात्मक और कम्प्यूटेशनल अध्ययन ने निष्कर्ष निकाला कि चयनित तीन एसआईटी ज्यामिति में से, कुल मिलाकर सबसे अच्छा एसआईटी का आकार आयताकार है, जो तलछट कणों के अधिक अंश को फंसा लेता है जिससे अधिकतम कण जाल दक्षता प्राप्त होती। ०.१५ मीटर और ०.०३ मीटर आकार के दो स्लॉट एपर्चर में से ०.१५ मीटर के स्लॉट एपर्चर आकार का उपयोग वर्तमान अध्ययन में शामिल प्रत्येक आयताकार एसआईटी की गहराई (y) की पूरी श्रृंखला में अधिकतम कण जाल दक्षता प्रदान करता है, जिसका उपयोग हाइड्रोलिक डिजाइन इंजीनियरों द्वारा मौजूदा या नए स्टार्मवाटर सीवर और शहरी खुले चैनल ड्रेनेज में अमल में लाया जा सकता है। आयताकार एसआईटी की विभिन्न गहराई, सीवर तलछट आकार श्रेणियों, प्रवाह गहराई और स्लॉट एपर्चर आकार के साथ कण ट्रेप दक्षता की भिन्नता के सावधानीपूर्वक विश्लेषण के आधार पर, ०.१५ मीटर के स्लॉट एपर्चर आकार के साथ $0.3\text{L} \leq y \leq 0.6\text{L}$ मीटर की सीमा में आयताकार एसआईटी की गहराई (y) और ०.०३ मीटर के स्लॉट एपर्चर आकार के साथ ०.३८ मीटर के बराबर आयताकार एसआईटी की गहराई (y) का उपयोग करने का सुझाव दिया

गया है। बॉटम-फिटेड एसआईटी के साथ एक खुले चैनल में प्रवाह के मॉडलिंग के लिए सबसे उपयुक्त सिमुलेशन मॉडल वीओएफ और रियालाइज़िबिल $k-\epsilon$ टरबुलेंस मॉडल हैं।

CONTENTS

<i>Certificate</i>	i
<i>Acknowledgement</i>	ii
<i>Abstract</i>	iv
<i>Contents</i>	xvi
<i>List of Figures</i>	xxiii
<i>List of Tables</i>	xxxvii
<i>List of Symbols</i>	xxxix
<i>List of Abbreviations</i>	xliii
Chapter 1 Introduction	
1.0 Background and motivation	1
1.1 Research gaps	14
1.2 Research objectives	17
1.3 Research flow chart	18
1.4 Scope of the present research work	19
1.5 Thesis organization	20
Chapter 2 Literature Review	
2.0 Introduction	22
2.1 Published studies	23
2.2 Urban drainage system	49
2.3 Sewer sediment	49
2.4 Impacts and causes of sewer sediment	49
2.4.1. Designing combined sewers with hydraulic systems	50
2.4.2. Re-entrainment of sediments that have been settled	50
2.4.3. The issue of structural disintegration and odor	50
2.4.4. The biological consequences	51
2.5 Sewer sediment management and control	51
2.5.1. All-inclusive approach	51
2.5.1.1. Management of solid-source	51
2.5.1.2. Inline and in-sewer control	51
2.5.1.3. Medical rehabilitation facilities	52
2.5.2. Physical or conventional techniques for sewer cleaning	52
2.5.2.1. Power rodding	52
2.5.2.2. Balling	53
2.5.2.3. Jetting	53
2.5.2.4. The concept of pigging	53
2.5.2.5. Power bucket	53
2.5.3. Sewer flushing	54
2.5.3.1. The process of flushing for sewer cleaning	55

2.5.3.2. Hydrass gate	55
2.5.3.3. Hydrosel self gate	56
2.5.3.4. A vacuum flushing system BIOGEST	57
2.5.4. Domestic approaches	58
2.5.5. Silt and sediment traps	58
2.5.5.1. Grit chambers, settling tanks and storage tanks	59
2.5.5.2. Sediment invert traps (SITs) for silt and bed load trapping	63
2.5.5.3. Superiority of sediment invert trap (SIT) over grit chamber and storage tank	67
2.6 Particle trap efficiency (I) of sediment invert trap (SIT)	68
2.7 Sediment transportation	69
2.8 Sediment	69
2.9 Origin and formation of sediments	69
2.10 Formation of sediments	70
2.10.1. Physical Weathering	70
2.10.2. Chemical Weathering	70
2.10.3. Mechanical Weathering	70
2.10.4. Organic Weathering	71
2.11 Characteristics of sediment (individual properties)	71
2.11.1. Sediment size	71
2.11.1.2. Nominal diameter or equivalent diameter	71
2.11.1.3. Fall diameter	71
2.11.1.4. Sedimentation diameter	72
2.11.1.5. Sieve diameter	72
2.11.2. Sediment shape	72
2.11.3. Sediment fall velocity (w_s)	73
2.11.4. Sediment orientation	74
2.11.4.1. Instantaneous orientation	74
2.11.4.2. Fabric orientation	75
2.11.5. Sediment density	75
2.12 Bulk properties of sediments	75
2.12.1. Particle size distribution	75
2.12.2. Standard deviation (σ)	75
2.12.3 Mode	76
2.12.4. Median size d_{50}	76
2.12.5. Porosity (P)	76
2.12.6. Specific weight (w)	76
2.12.7. Angle of repose (ψ)	77
2.13 Movement of sediment particles in an open channel flow	77
2.13.1. Incipient motion of sediment particles	77
2.13.1.1. Competency velocity concept	78
2.13.1.2. Lift concept	78

2.13.1.3. Critical tractive force concept	78
2.13.2. Shields analysis	78
2.14 Bed forms	79
2.14.1. Plane bed without motion of sediment particles	80
2.14.2. Ripple and dunes	80
2.14.3. Transition bed forms	81
2.14.3.1. Plane bed with sediment motion	81
2.14.3.2. Standing wave	82
2.14.4. Antidunes	82
2.15 Modes of sediment transport	83
2.15.1. Bed load transport and saltation	83
2.15.2. Mechanism of Saltation	84
2.15.3. Modes of sediment transport defined by subcommittee of AGU	85
2.15.3.1. Contact load	85
2.15.3.2. Saltation load	85
2.15.3.3. Bed load	86
2.15.3.4. Suspended load	86
2.15.3.5. Total load	87
2.15.3.6. Wash load	87
2.16 Sediment transport in urban drainage system	87
Chapter 3 Theory and Computational Fluid Dynamics (CFD) Formulations of Simulation Models Used in the Present Study	
3.0 Introduction	89
3.1 Euler-Euler technique	90
3.1.1 Volume of fluid (VOF) model	92
3.1.2 Mixture model	92
3.1.3 Eulerian model	93
3.2 Formulations of VOF model	93
3.2.1. The equation of continuity	94
3.2.3. The equation of momentum	94
3.2.3. Surface tension prediction	94
3.2.4. Open channel flow	95
3.3 Turbulence, turbulent flow and turbulence model	96
3.3.1. Characteristics of turbulent flow	97
3.3.2. Causes of turbulence in a flow	100
3.3.3. Types of turbulent flows	103
3.3.4. Turbulent flow representation	104
3.3.5. Turbulence model	106
3.3.6. Turbulence kinetic energy	107
3.3.7. Functions for the wall treatment	112

3.3.8. Near wall cell size	113
3.3.9. Turbulence and its role in particle entrainment	113
3.3.9.1. Mechanism of suspension of sediment particle due to turbulence	119
3.4 Discrete phase model (DPM)	128
3.4.1. One-way and two-way coupling	124
3.5 Meshing	129
3.5.1. Grid cell quality	129
3.5.1.1 The orthogonal quality	129
3.5.1.2. The concept of aspect ratio	130
3.5.1.3. The concept of skewness	130
Chapter 4 Measurement of Velocity Distribution Inside Open Channel and Sediment Invert Traps (SITs) Using Two-Dimensional Particle Image Velocimetry (2D-PIV)	
4.0 Introduction	132
4.1 Particle image velocimetry (PIV)	134
4.2 Materials and methodology	136
4.3 Velocity measurement procedure using PIV and apparatus detail	137
4.4 Results and discussion of velocity measurements in open channel flume	139
4.5 Results and discussion of velocity measurements inside sediment invert traps at slot size (x) = 0.15 m	149
4.5.1. Velocity variation with respect to depths of SIT	154
4.5.2. Velocity variation with respect to flow depths	155
4.5.3. Velocity variation with respect to shape of SIT	155
4.6 Effect of single-pass and multi-pass cross correlation methods on velocity distribution inside sediment invert traps	155
4.7 Conclusions	159
Chapter 5 Case Study: Significance of Including Lid-Thickness and Particle Shape Factor in Numerical Modeling for Prediction of Particle Trap Efficiency of Invert Trap	
5.0 Introduction	164
5.1 Input data	168
5.2 Mode of sediment movement in flume	169
5.3 Measurement of velocity distribution using 2D PIV	169
5.4 Determination of particle shape factor	171
5.5 Numerical modeling strategies	173
5.6 Geometry creation and grid generation	174
5.7 Numerical models used in this study	176
5.7.1 VOF model	176
5.7.2 Realizable k - ε turbulence model	176
5.7.3 DPM	177

5.7.4	Model boundary conditions and settings	179
5.8	Results and discussion	181
5.8.1	Particle trap efficiency of invert trap	181
5.8.2	Effect of lid thickness	183
5.8.3	Effect of particle shape factor	185
5.8.4	Velocity distribution inside irregular hexagonal invert trap	187
5.8.5	Profile of free water surface	188
5.9	Numerically simulated trap efficiency variation with extra set of lid thicknesses (t)	191
5.10	Conclusions	199
Chapter 6	Experimental Programme to Measure Particle Trap Efficiency of Sediment Invert Traps (SITs)	
6.0	Introduction	201
6.1	Apparatus details	201
6.1.1	Open channel flume	202
6.1.2	Sediment invert trap (SIT)	202
6.1.3	Lids and slot aperture	206
6.1.4	Sediment injector	207
6.1.5	Inlet tank	207
6.1.6	Storage tank	208
6.1.7	Water pump	208
6.1.8	Flow meter	208
6.1.9	Discharge valve	208
6.1.10	Channel bed slope and it's changing mechanism	208
6.2	Sediment parameters	209
6.2.1	Type of sediments	209
6.2.2	Particle size distribution (PSD) analysis	214
6.2.3	Specific gravity (G) and density of sewer solid (ρ_{ss})	215
6.2.4	Sedimentation parameter (S_p) and sewer sediment particle size range selection	216
6.2.5	Sewer sediment shape	217
6.2.6	Shape factor	220
6.3	Flow Properties	223
6.4	Experimental procedure	223
Chapter 7	Two- and Three-Dimensional (2D and 3D) Simulation Modeling Set-Up to Predict Particle Trap Efficiency of Sediment Invert Traps (SITs)	
7.0	Introduction	227
7.1	Numerical model set-up	229
7.1.1.	Two- and three-dimensional geometry of flow domain	230
7.1.2.	Two- and three-dimensional grid generation for flow domain	238

7.1.2.1. Two-dimensional (2D) grid generation	238
7.1.2.2. Three-dimensional (3D) grid generation	241
7.1.3. Flow model boundary conditions and parameter settings for 2D and 3D simulations	248
7.1.4. Turbulence model boundary conditions and parameter settings for 2D and 3D simulations	249
7.1.5. Discrete phase model (DPM) boundary conditions and parameter settings for 2D and 3D simulations	250
7.1.6. Solution methods for 2D and 3D simulations	254
7.1.7. Solution control for 2D and 3D simulations	256
7.1.8. Solution initialization for 2D and 3D simulations	257
7.1.9. Residual monitoring and solution convergence criteria for 2D and 3D simulations	258
Chapter 8 Results, Analysis, Discussions, Comparisons and Validations	
8.0 Introduction	259
8.1 Results and Analysis	259
8.2 Discussion and comparison between 2D and 3D predicted particle trap efficiency of sediment invert trap (SIT)	279
8.3 Effect of depth of flow (Y) on particle trap efficiency of sediment invert trap (SIT)	285
8.4 Effect of particle shape (in terms of shape factor ϕ) on particle trap efficiency of SIT	292
8.5 Effect of shape of sediment invert trap (SIT) on particle trap efficiency	295
8.6 Effect of slot aperture size (x) on particle trap efficiency of sediment invert trap (SIT)	295
8.7 Effect of sediment size on particle trap efficiency of sediment invert trap (SIT)	301
8.8 Effect of depth of sediment invert trap (y) on particle trap efficiency of sediment invert trap (SIT)	307
8.9 Particle deposition pattern in sediment invert traps (SITs)	316
8.10 Velocity distribution in sediment invert traps (SITs)	323
8.11 Free water surface profile validation	361
8.12 Velocity validation in open channel flume and sediment invert traps (SITs)	368
8.12.1. Velocity validation in open channel flume	368
8.12.2. Velocity validation inside sediment invert traps (SITs) at slot aperture size (x) = 0.15 m	371
8.12.2.1. Rectangular SIT	373
8.12.2.2. Irregular hexagonal SIT	373
8.12.2.3. Trapezoidal SIT	373
8.12.3. Effect of single-pass and multi-pass cross correlation methods on velocity distribution inside sediment invert traps (SITs)	376

Chapter 9	Development of An Empirical Regression Model to Predict Particle Trap Efficiency of Sediment Invert Traps (SITs) Using Generalized Reduced Gradient (GRG) Non-Linear Iterative Solver	
9.0	Introduction	381
9.1	Dimensional analysis	381
9.2	Dimensions	382
9.3	Dimensional homogeneity	382
9.4	Methods of dimensional analysis	382
	9.4.1. Buckingham's π -method	383
9.5	Dimensional analysis for the present study	384
9.6	Regression analysis and its types	387
	9.6.1. Linear regression	388
	9.6.2. Non-linear regression	389
	9.6.3. Methods of determining regression coefficients	391
	9.6.3.1. Least square method for determining regression coefficients of linear regression models	391
	9.6.3.2. Least square method for determining regression coefficients of non-linear regression models	392
9.7	Microsoft Excel SOLVER and Generalized Reduced Gradient (GRG) method	393
9.8	Regression model performance indicators	394
9.9	Regression analysis for the present study	396
9.10	Sensitivity analysis	408
9.11	Results and discussion	409
9.12	Conclusions	415
Chapter 10	Conclusions and Scope for the Future Study	
10.0	Conclusions	417
10.1	Scope for the future study	420
References		422
Publications Out of the Present Study		455
Brief Bio-Data		456

LIST OF FIGURES

Fig. 1.1	Sediments entering from road into the stormwater drain inlet in IIT Delhi campus, India (2016)	2
Fig. 1.2	Movement of sediments in a circular sewer as bed load and suspended load	2
Fig. 1.3	Deposited sediments in an unlined irrigation canal	3
Fig. 1.4	Settled sediment in open rectangular stormwater sewer	4
Fig. 1.5	Water logging in front of the entrance gate of Kumaon hostel after rainfall in IIT Delhi campus, New Delhi, India (2019)	4
Fig. 1.6	Water logging on roads and streets after rainfall in different areas of New Delhi, India	5
Fig. 1.7	Research flow chart	18
Fig. 2.1	An apparatus used by Poreh <i>et al.</i> 1970	24
Fig. 2.2	Functioning stages of Hydrass gate	55
Fig. 2.3	Hydroself gate	56
Fig. 2.4	Flushing gate	57
Fig. 2.5	Traditional French grit chamber	61
Fig. 2.6a	On-line sewer sediment storage tank	63
Fig. 2.6b	Line diagram of European on-line and off-line storage tanks	63
Fig. 2.7	A 2D diagram of the French sediment invert trap used in Marseilles	64
Fig. 2.8	Chart for determination of sphericity of coarse particles	73
Fig. 2.9	Particle size distribution curve for the sediment	75
Fig. 2.10	Illustration of Hiding and exposure effects in case of non-uniform sediments	77
Fig. 2.11	Shields' diagram	79
Fig. 2.12	Ripples	80
Fig. 2.13	Dunes	81
Fig. 2.14a	Washed-out dunes	81
Fig. 2.14b	Plane bed with sediment motion	82
Fig. 2.15	Standing wave	82
Fig. 2.16	Antidune	83
Fig. 2.17	Processes of erosion, transport and sedimentation	84
Fig. 2.18	Four illustrated positions of saltating particles	85
Fig. 2.19	Forces acting on a saltating particle in position 2	85

Fig. 2.20	Successive positions of saltating particle before it loses contact with the bed	85
Fig. 2.21	Definition sketch of the bed & suspended load layer	86
Fig. 3.1	Profiles of average velocity (\bar{u}) and turbulent strength (u_{rms}) in open channel	98
Fig. 3.2	Profiles of average velocity (\bar{u}) and turbulence strength (u_{rms}) in a jet	99
Fig. 3.3	Turbulence and shear stress over the wall	100
Fig. 3.4	Turbulence and shear stress in a jet	100
Fig. 3.5	Turbulence and shear stress in the slot aperture region of SIT	101
Fig. 3.6	Instantaneous production of turbulence (eddies) in a pipe flow	102
Fig. 3.7	Generation of eddies due to turbulence in a flow	102
Fig. 3.8	External wall turbulent shear flows in (a) Open channel (b) Flow past a step	103
Fig. 3.9	Internal wall turbulent shear flows in (a) Pipes (b) Bends	103
Fig. 3.10	Jet which is affected by boundary	104
Fig. 3.11	Representation of Reynolds decomposition which splits the turbulent flow properties into a statistical mean and a statistically fluctuating component	104
Fig. 3.12	Shields' diagram	116
Fig. 3.13	Structure and motion of an eddy in turbulent boundary layer region near the wall	120
Fig. 3.14	Turbulent bursting mechanism depicting ejection and sweep; flow is from left to right and the length of the arrow depicts the relative velocity in the velocity profiles	123
Fig. 3.15	Computational vectors for cell orthogonal quality (ANSYS Fluent 2020 R1)	130
Fig. 3.16	Triangles and quadrilaterals (ideal and skewed)	131
Fig. 4.1	Working diagram of PIV (rtCam PIV System Manual 2009)	134
Fig. 4.2	Symbolic diagram showing post processing of PIV software (rtCam PIV System Manual 2009)	135
Fig. 4.3	3D diagram of physical model used for PIV measurements	138
Fig. 4.4	2D PIV measured velocity profiles in open channel flume at average flow velocity (V) = 0.677 m/s (flow depth, Y = 0.02 m)	139
Fig. 4.5	2D PIV measured velocity profiles in open channel flume at average flow velocity (V) = 0.913 m/s (flow depth, Y = 0.04 m)	140
Fig. 4.6	2D PIV measured velocity profiles in open channel flume at average flow velocity (V) = 0.975 m/s (flow depth, Y = 0.06 m)	140

Fig. 4.7	Vertical streamwise velocity profiles at the centre of the flume at a distance of 2.5 m from the flume's inlet at: (a) Y or $h = 0.02$ m (b) Y or $h = 0.04$ m (c) Y or $h = 0.06$ m	146
Fig. 4.8	Locations at section ZZ at which vertical streamwise velocity was measured and predicted: (a) Horizontal plan view (b) Vertical cross section across half of the width of the flume	147
Fig. 4.9	Vertical streamwise velocity profiles at lateral distances z_1 to z_4 from the flume's side wall to the flume's centre line predicted by Eq. (4.3) at a distance of 2.5 m from the flume's inlet: (a) at Y or $h = 0.02$ m (b) at Y or $h = 0.04$ m (c) at Y or $h = 0.06$ m	148
Fig. 4.10	PIV measured velocity vector field at flow depth (Y) = 0.02 m and slot size (x) = 0.15 m in rectangular SIT of depth: (a) $y = 0.23$ m (b) $y = 0.28$ m (c) $y = 0.33$ m (d) $y = 0.38$ m	151
Fig. 4.11	PIV measured velocity vector field in rectangular SIT of depth (y) = 0.23 m and slot size (x) = 0.15 m at flow depths: (a) $Y = 0.04$ m (b) $Y = 0.06$ m	151
Fig. 4.12	PIV measured velocity vector field at flow depth (Y) = 0.02 m and slot size (x) = 0.15 m in irregular hexagonal SIT of depth: (a) $y = 0.23$ m (b) $y = 0.28$ m (c) $y = 0.33$ m (d) $y = 0.38$ m	152
Fig. 4.13	PIV measured velocity vector field in irregular hexagonal SIT of depth (y) = 0.23 m and slot size (x) = 0.15 m at flow depths: (a) $Y = 0.04$ m (b) $Y = 0.06$ m	152
Fig. 4.14	PIV measured velocity vector field at flow depth (Y) = 0.02 m and slot size (x) = 0.15 m in trapezoidal SIT of depth: (a) $y = 0.23$ m (b) $y = 0.28$ m (c) $y = 0.33$ m (d) $y = 0.38$ m	153
Fig. 4.15	PIV measured velocity vector field in trapezoidal SIT of depth (y) = 0.23 m and slot size (x) = 0.15 m at flow depths: (a) $Y = 0.04$ m (b) $Y = 0.06$ m	153
Fig. 4.16	Effect of single-pass and multi-pass cross correlation methods on velocity vector field and pattern of flow structures with respect to depth of SIT (y) in rectangular SIT with slot size (x) = 0.15 m at: (a) $Y = 0.02$ m, $y = 0.28$ m (b) $Y = 0.02$ m, $y = 0.33$ m	158
Fig. 4.17	Effect of single-pass and multi-pass cross correlation methods on velocity vector field and pattern of flow structures with respect to flow depth (Y) in rectangular SIT with slot size (x) = 0.15 m at: (a) $Y = 0.02$ m, $y = 0.28$ m (b) $Y = 0.04$ m, $y = 0.28$ m	159
Fig. 5.1	3D diagram of physical model used for PIV measurements	169
Fig. 5.2	SEM and binary images of actual sewer particles in sizes of 150 to 300 μm and 300 to 425 μm at 55 times of magnification and 200-mm scale for particle shape factor determination.	172
Fig. 5.3	3D geometry of flume, invert trap, and lids created in Space Claim for numerical modeling with flow depth of 0.01 m	175

Fig. 5.4	Variation of TKE along horizontal line between top edges of upstream and downstream lids: (a) with no consideration of lid thickness ($t = 0$ m) and (b) with consideration of lid thickness ($t = 0.016$ m) (flow is from left to right)	184
Fig. 5.5	Particle paths tracked by DPM with $Y = 0.05$ m, $x = 0.15$ m, $y = 0.28$ m, and $t = 0$ m (flow is from left to right)	186
Fig. 5.6	Particle paths tracked by DPM with $Y = 0.05$ m, $x = 0.15$ m, $y = 0.28$ m, and $t = 0.016$ m (flow is from left to right)	186
Fig. 5.7	Velocity vector fields: (a) prediction of Mohsin and Kaushal (2017) with $t = 0$ m; (b) prediction of this study with $t = 0.016$ m; and (c) measurement in this study with $t = 0.016$ m with $Y = 0.05$ m, $x = 0.15$ m, and $y = 0.28$ m (flow is from left to right)	187
Fig. 5.8	Velocity distribution profile in flume at a distance of 2.5 m from flume inlet at 0.05 m flow depth (flow is from left to right)	188
Fig. 5.9	Water surface profiles with flow depth of 0.02 m. (a) VOF-predicted water surface profile with $t = 0$ m, (b) VOF-predicted water surface profile with $t = 0.016$ m, and (c) experimental water surface profile with $t = 0.016$ m	189
Fig. 5.10	Simulated water surface profiles at $Y = 0.01, 0.02, 0.03, 0.04$ and 0.05 m, $x = 0.15$ m, $y = 0.28$ m (a) Without upstream and downstream lid thickness; $t = 0$ m (b) With upstream and downstream lid thickness; $t = 0.016$ m [flow is from left to right]	190
Fig. 5.11	Variation of simulated particle trap efficiency relative to lid thicknesses at all five depths of flow with (a) Particle size range R_1 (b) Particle size range R_2	192
Fig. 5.12	Variation of turbulent kinetic energy along the horizontal line between top edge of upstream and downstream lids (a) with lid-thickness; $t = 0.032$ m (b) with lid-thickness; $t = 0.048$ m [flow is from left to right]	193
Fig. 5.13	Velocity distribution inside invert trap and flume with lid thickness $t = 0$ m and slot width (x) of 0.15 m at: (a) Depth of flow (Y) = 0.01 m (b) Depth of flow (Y) = 0.02 m (c) Depth of flow (Y) = 0.03 m (d) Depth of flow (Y) = 0.04 m (e) Depth of flow (Y) = 0.05 m [flow is from left to right]	194
Fig. 5.14	Velocity distribution inside invert trap and flume with lid thickness $t = 0.016$ m and slot width (x) of 0.15 m at: (a) Depth of flow (Y) = 0.01 m (b) Depth of flow (Y) = 0.02 m (c) Depth of flow (Y) = 0.03 m (d) Depth of flow (Y) = 0.04 m (e) Depth of flow (Y) = 0.05 m [flow is from left to right]	195
Fig. 5.15	Velocity distribution inside invert trap and flume with lid thickness $t = 0.032$ m and slot width (x) of 0.15 m t (a) Depth of flow (Y) = 0.01 m (b) Depth of flow (Y) = 0.02 m (c) Depth of flow (Y) = 0.03 m (d) Depth	196

	of flow (Y) = 0.04 m (e) Depth of flow (Y) = 0.05 m [flow is from left to right]	
Fig. 5.16	Velocity distribution inside invert trap and flume with lid thickness $t = 0.048$ m and slot width (x) of 0.15 m at: (a) Depth of flow (Y) = 0.01 m (b) Depth of flow (Y) = 0.02 m (c) Depth of flow (Y) = 0.03 m (d) Depth of flow (Y) = 0.04 m (e) Depth of flow (Y) = 0.05 m [flow is from left to right]	197
Fig. 5.17	Simulated water surface profiles (for extra lid thicknesses) at $Y = 0.01, 0.02, 0.03, 0.04$ and 0.05 m, $x = 0.15$ m, $y = 0.28$ m (a) With upstream and downstream lid thickness; $t = 0.032$ m (b) With upstream and downstream lid thickness; $t = 0.048$ m [flow is from left to right]	198
Fig. 5.18	Particles path tracked by DPM at $Y = 0.05$ m, $x = 0.15$ m, $y = 0.28$ m and $t = 0.032$ m (flow is from left to right)	199
Fig. 5.19	Particles path tracked by DPM at $Y = 0.05$ m, $x = 0.15$ m, $y = 0.28$ m and $t = 0.048$ m (flow is from left to right)	199
Fig. 6.1	3D layout of the physical model	204
Fig. 6.2	Laboratory view of an experimental set-up	205
Fig. 6.3	View of slot widths (x) and lids over the rectangular SIT	206
Fig. 6.4	View of slot widths (x) and lids over the irregular hexagonal SIT	206
Fig. 6.5	View of slot widths (x) and lids over the trapezoidal SIT	207
Fig. 6.6	Sediment injector (Mohsin and Kaushal 2017)	207
Fig. 6.7	Sewer sediment sample (SS_1) collection from rectangular open storm sewer drain (surface drain) located in the residential area in the district Aligarh, Uttar Pradesh, India (17 Dec. 2018)	211
Fig. 6.8	Sewer sediment sample (SS_2) collection from unlined rectangular open storm sewer drain (collecting combined sewage flows) located along the highway side in the district Aligarh, Uttar Pradesh, India (17 Dec. 2018)	212
Fig. 6.9	Dried sewer sediments of size ranges 0.850 to 425 μ m, 0.425 to 0.212 mm and 0.212 to 0.150 mm from sewer sediment sample SS_1	213
Fig. 6.10	Dried sewer sediments of size ranges 0.425 to 0.212 mm and 0.212 to 0.150 mm from sewer sediment sample SS_2	214
Fig. 6.11	PSD of sewer sediment samples SS_1 and SS_2	215
Fig. 6.12a	SEM images of 20 randomly selected sewer sediment particles present in the size range SS_1SR_1 (850 - 425 μ m) from sewer sediment sample SS_1 at 57x magnification and a 200 μ m scale	218
Fig. 6.12b	SEM images of 48 randomly selected sewer sediment particles present in the size range SS_1SR_2 (425 - 212 μ m) from sewer sediment sample SS_1 at 57x magnification and a 200 μ m scale	218

Fig. 6.12c	SEM images of 72 randomly selected sewer sediment particles present in the size range SS ₁ SR ₃ (212 - 150 μm) from sewer sediment sample SS ₁ at 57x magnification and a 200 μm scale	219
Fig. 6.13a	SEM images of 6 randomly selected sewer sediment particles present in the size range SS ₂ SR ₁ (425 - 212 μm) from sewer sediment sample SS ₂ at 55x magnification and a 200 μm scale	219
Fig. 6.13b	SEM images of 10 randomly selected sewer sediment particles present in the size range SS ₂ SR ₂ (212 - 150 μm) from sewer sediment sample SS ₂ at 55x magnification and a 200 μm scale	219
Fig. 6.14	Flow depth vs discharge curve	223
Fig. 7.1a	The 2D geometry of an open channel flume and rectangular SIT with u/s and d/s lids for 2D CFD simulations	232
Fig. 7.1b	The 2D geometry of an open channel flume and irregular hexagonal SIT with u/s and d/s lids for 2D CFD simulations	233
Fig. 7.1c	The 2D geometry of an open channel flume and trapezoidal SIT with u/s and d/s lids for 2D CFD simulations	234
Fig. 7.2a	The 3D geometry of an open channel flume and rectangular SIT with u/s and d/s lids for CFD simulations	235
Fig. 7.2b	The 3D geometry of an open channel flume and irregular hexagonal SIT with u/s and d/s lids for CFD simulations	236
Fig. 7.2c	The 3D geometry of an open channel flume and trapezoidal SIT with u/s and d/s lids for CFD simulations	237
Fig. 7.3	Average velocity in an open channel measured by EMF and predicted by VOF model with $k-\epsilon$ (realizable) and $k-\omega$ (SST) turbulence models at 0.02, 0.04 and 0.06 m flow depths (Y) in case of 2D simulation	239
Fig. 7.4	Quadrilateral mesh of 0.002 m grid/cell size for the whole flow domain with slot aperture (x) = 0.15m	240
Fig. 7.5	Average velocity in an open channel measured by EMF and predicted by VOF model with $k-\epsilon$ (realizable) and $k-\omega$ (SST) turbulence models at 0.02, 0.04 and 0.06 m flow depths (Y) in case of 3D simulation	242
Fig. 7.6a	Hexahedral mesh of 0.003 m grid/cell size in the region of the flow domain from the bottom of the SIT upto the free water surface for 0.02 m flow depth (Y) in one of the cases of rectangular SIT.	245
Fig. 7.6b	Hexahedral mesh of 0.003 m grid/cell size in the region of the flow domain from the bottom of the SIT upto the free water surface for 0.04 m flow depth (Y) in one of the cases of rectangular SIT.	246
Fig. 7.6c	Hexahedral mesh of 0.003 m grid/cell size in the region of the flow domain from the bottom of the SIT upto the free water surface for 0.06 m flow depth (Y) in one of the cases of rectangular SIT.	247

Fig. 7.7	Particle injection and its movement simulated by DPM in open channel and rectangular SIT at slot aperture of 0.03 m	253
Fig. 8.1	Comparison between experimental and numerically predicted trap efficiencies; (a) 2D simulation with non-spherical particles in DPM (b) 2D simulation with spherical particles in DPM (c) 3D simulation with non-spherical particles in DPM (d) 3D simulation with spherical particles in DPM [in case of rectangular SIT]	276
Fig. 8.2	Comparison between experimental and numerically predicted trap efficiencies; (a) 2D simulation with non-spherical particles in DPM (b) 2D simulation with spherical particles in DPM (c) 3D simulation with non-spherical particles in DPM (d) 3D simulation with spherical particles in DPM [in case of irregular hexagonal SIT]	277
Fig. 8.3	Comparison between experimental and numerically predicted trap efficiencies; (a) 2D simulation with non-spherical particles in DPM (b) 2D simulation with spherical particles in DPM (c) 3D simulation with non-spherical particles in DPM (d) 3D simulation with spherical particles in DPM [in case of trapezoidal SIT]	278
Fig. 8.4	Variation of TKE along horizontal lines (XX, AB, CD, EF, GH) between top edges of upstream and downstream lids in: (a) 2D simulation (b) 3D simulation; in rectangular SIT with depth of SIT (y) = 0.38 m, flow depth (Y) = 0.02 m and slot aperture size (x) = 0.15 m [flow is from left to right].	282
Fig. 8.5	Variation of TKE along horizontal lines (XX, AB, CD, EF, GH) between top edges of upstream and downstream lids in: (a) 2D simulation (b) 3D simulation; in rectangular SIT with depth of SIT (y) = 0.38 m, flow depth (Y) = 0.04 m and slot aperture size (x) = 0.15 m [flow is from left to right].	283
Fig. 8.6	Variation of TKE along horizontal lines (XX, AB, CD, EF, GH) between top edges of upstream and downstream lids in: (a) 2D simulation (b) 3D simulation; in rectangular SIT with depth of SIT (y) = 0.38 m, flow depth (Y) = 0.06 m and slot aperture size (x) = 0.15 m [flow is from left to right].	284
Fig. 8.7	Variation of experimental and predicted (2D and 3D simulations with spherical particles in DPM) particle trap efficiencies with varied depths of flow (Y) at slot aperture x = 0.15 m for all depths of SIT (y) with sewer sediment size range SS_1SR_1 in rectangular SIT	285
Fig. 8.8	Variation of experimental and predicted (2D and 3D simulations with non-spherical particles in DPM) particle trap efficiencies with varied depths of flow (Y) at slot aperture x = 0.15 m for all depths of SIT (y) with sewer sediment size range SS_1SR_1 in rectangular SIT	286
Fig. 8.9	Variation of experimental and predicted (2D and 3D simulations with spherical particles in DPM) particle trap efficiencies with varied depths of flow (Y) at slot aperture x = 0.03 m for all depths of SIT (y) with sewer sediment size range SS_1SR_1 in rectangular SIT	286

- Fig. 8.10 Variation of experimental and predicted (2D and 3D simulations with non-spherical particles in DPM) particle trap efficiencies with varied depths of flow (Y) at slot aperture $x = 0.03$ m for all depths of SIT (y) with sewer sediment size range SS_1SR_1 in rectangular SIT 287
- Fig. 8.11 TKE variation along the vertical line at the centre of a 0.23 m deep rectangular SIT with slot aperture of 0.15 m at flow depths of (a) $Y = 0.02$ m; (b) $Y = 0.04$ m; (c) $Y = 0.06$ m [flow is from left to right] 289
- Fig. 8.12 TKE variation along the vertical line at the centre of a 0.23 m deep rectangular SIT with slot aperture of 0.03 m at flow depths of (a) $Y = 0.02$ m; (b) $Y = 0.04$ m; (c) $Y = 0.06$ m [flow is from left to right] 289
- Fig. 8.13 Variation of particle velocity with increased depth of flow at slot aperture (x) = 0.15 m, depth of SIT (y) = 0.23 m, and particle size range SS_1SR_1 [flow is from left to right] 291
- Fig. 8.14 2D predicted variation of particle trap efficiency with particle shape (shape factor $\phi = 0.41$) in rectangular SIT with sewer sediment size range SS_1SR_1 at: (a) slot aperture $x = 0.15$ m (b) slot aperture $x = 0.03$ m; at flow depth of 0.02, 0.04 and 0.06 m 293
- Fig. 8.15 3D predicted variation of particle trap efficiency with particle shape (shape factor $\phi = 0.41$) in rectangular SIT with sewer sediment size range SS_1SR_1 at: (a) slot aperture $x = 0.15$ m (b) slot aperture $x = 0.03$ m; at flow depth of 0.02, 0.04 and 0.06 m 294
- Fig. 8.16 Experimentally measured and 2D and 3D CFD predicted variation of particle trap efficiency with slot aperture (x) for sewer sediment size range SS_1SR_1 at flow depths: (a) $Y = 0.02$ m (b) $Y = 0.04$ m (c) $Y = 0.06$ m (in rectangular SITs of depths y) 297
- Fig. 8.17 Experimentally measured and 2D and 3D CFD predicted variation of particle trap efficiency with slot aperture (x) for sewer sediment size range SS_1SR_1 at flow depths: (a) $Y = 0.02$ m (b) $Y = 0.04$ m (c) $Y = 0.06$ m (in trapezoidal SITs of depths y) 298
- Fig. 8.18 Experimentally measured and 2D and 3D CFD predicted variation of particle trap efficiency with slot aperture (x) for sewer sediment size range SS_1SR_1 at flow depths: (a) $Y = 0.02$ m (b) $Y = 0.04$ m (c) $Y = 0.06$ m (in irregular hexagonal SITs of depths y) 299
- Fig. 8.19 Experimentally measured and 2D and 3D CFD predicted variation of particle trap efficiency with slot aperture (x) for sewer sediment size range SS_1SR_3 at flow depths: (a) $Y = 0.02$ m (b) $Y = 0.04$ m (c) $Y = 0.06$ m (in irregular hexagonal SITs of depths y) 300
- Fig. 8.20 Variation of particle trap efficiency with sewer sediment size ranges at 0.02 m flow depth and 0.15 m slot aperture size: (a) Experimentally measured (b) Predicted by 2D simulations (c) Predicted by 3D simulations (in rectangular SITs of depths y) 303

- Fig. 8.21 Variation of particle trap efficiency with sewer sediment size ranges at 0.02 m flow depth and 0.03 m slot aperture size: (a) Experimentally measured (b) Predicted by 2D simulations (c) Predicted by 3D simulations (in rectangular SITs of depths y) 304
- Fig. 8.22 Variation of particle trap efficiency with sewer sediment size ranges at 0.02 m flow depth and 0.15 m slot aperture size: (a) Experimentally measured (b) Predicted by 2D simulations (c) Predicted by 3D simulations (in irregular hexagonal SITs of depths y) 305
- Fig. 8.23 Variation of particle trap efficiency with sewer sediment size ranges at 0.04 m flow depth and 0.03 m slot aperture size: (a) Experimentally measured (b) Predicted by 2D simulations (c) Predicted by 3D simulations (in irregular hexagonal SITs of depths y) 306
- Fig. 8.24 3D predicted variation of particle trap efficiency with depth of SIT (y) for sewer sediment size ranges SS_1SR_1 , SS_1SR_2 , SS_1SR_3 , SS_2SR_1 and SS_2SR_2 at a slot aperture of: (a) $x = 0.15$ m (b) $x = 0.03$ m; at flow depths (Y) of 0.02, 0.04 and 0.06 m for rectangular SIT 310
- Fig. 8.25 3D predicted variation of particle trap efficiency with depth of SIT (y) for sewer sediment size ranges SS_1SR_1 , SS_1SR_2 , SS_1SR_3 , SS_2SR_1 and SS_2SR_2 at a slot aperture of: (a) $x = 0.15$ m (b) $x = 0.03$ m; at flow depths (Y) of 0.02, 0.04 and 0.06 m for irregular hexagonal SIT 311
- Fig. 8.26 3D predicted variation of particle trap efficiency with depth of SIT (y) for sewer sediment size ranges SS_1SR_1 , SS_1SR_2 , SS_1SR_3 , SS_2SR_1 and SS_2SR_2 at a slot aperture of: (a) $x = 0.15$ m (b) $x = 0.03$ m; at flow depths (Y) of 0.02, 0.04 and 0.06 m for trapezoidal SIT 312
- Fig. 8.27 2D-CFD simulated TKE contours inside rectangular SITs and variation of TKE along the vertical line at the center of SITs with a slot aperture size of 0.15 m and a flow depth of 0.02 m in depths of SIT: (a) $y = 0.23$ m; (b) $y = 0.28$ m; (c) $y = 0.33$ m; (d) $y = 0.38$ m; (e) $y = 0.43$ m; (f) $y = 0.48$ m; (g) $y = 0.53$ m; (h) $y = 0.58$ m; (i) $y = 0.65$ m; and (j) $y = 0.70$ m (flow is from left to right) 313
- Fig. 8.28 2D-CFD simulated TKE contours inside irregular hexagonal SITs and variation of TKE along the vertical line at the center of SITs with a slot aperture size of 0.15 m and a flow depth of 0.02 m in depths of SIT: (a) $y = 0.23$ m; (b) $y = 0.28$ m; (c) $y = 0.33$ m; (d) $y = 0.38$ m; (e) $y = 0.43$ m; (f) $y = 0.48$ m; (g) $y = 0.53$ m; (h) $y = 0.58$ m; (i) $y = 0.65$ m; and (j) $y = 0.70$ m (flow is from left to right) 314
- Fig. 8.29 2D-CFD simulated TKE contours inside trapezoidal SITs and variation of TKE along the vertical line at the center of SITs with a slot aperture size of 0.15 m and a flow depth of 0.02 m in depths of SIT: (a) $y = 0.23$ m; (b) $y = 0.28$ m; (c) $y = 0.33$ m; (d) $y = 0.38$ m; (e) $y = 0.43$ m; (f) $y = 0.48$ m; (g) $y = 0.53$ m; (h) $y = 0.58$ m; (i) $y = 0.65$ m; and (j) $y = 0.70$ m (flow is from left to right) 315

Fig. 8.30a	Particle deposition patterns for sewer sediment size range SS_1SR_1 in rectangular SITs at a flow depth of 0.02 m and slot aperture sizes of (a) $x = 0.15$ m; and (b) $x = 0.03$ m	317
Fig. 8.30b	Particle deposition patterns for sewer sediment size range SS_1SR_2 in rectangular SITs at a flow depth of 0.02 m and slot aperture sizes of (a) $x = 0.15$ m; and (b) $x = 0.03$ m	318
Fig. 8.30c	Particle deposition patterns for sewer sediment size range SS_1SR_3 in rectangular SITs at a flow depth of 0.02 m and slot aperture sizes of (a) $x = 0.15$ m; and (b) $x = 0.03$ m	318
Fig. 8.31a	Particle deposition patterns for sewer sediment size range SS_1SR_1 in irregular hexagonal SITs at a flow depth of 0.02 m and slot aperture sizes of (a) $x = 0.15$ m; and (b) $x = 0.03$ m	319
Fig. 8.31b	Particle deposition patterns for sewer sediment size range SS_1SR_2 in irregular hexagonal SITs at a flow depth of 0.02 m and slot aperture sizes of (a) $x = 0.15$ m; and (b) $x = 0.03$ m	320
Fig. 8.31c	Particle deposition patterns for sewer sediment size range SS_1SR_3 in irregular hexagonal SITs at a flow depth of 0.02 m and slot aperture sizes of (a) $x = 0.15$ m; and (b) $x = 0.03$ m	320
Fig. 8.32a	Particle deposition patterns for sewer sediment size range SS_1SR_1 in trapezoidal SITs at a flow depth of 0.02 m and slot aperture sizes of (a) $x = 0.15$ m; and (b) $x = 0.03$ m	321
Fig. 8.32b	Particle deposition patterns for sewer sediment size range SS_1SR_2 in trapezoidal SITs at a flow depth of 0.02 m and slot aperture sizes of (a) $x = 0.15$ m; and (b) $x = 0.03$ m	322
Fig. 8.32c	Particle deposition patterns for sewer sediment size range SS_1SR_3 in trapezoidal SITs at a flow depth of 0.02 m and slot aperture sizes of (a) $x = 0.15$ m; and (b) $x = 0.03$ m	322
Fig. 8.33	Numerically simulated velocity distribution inside rectangular SIT with depth of flow (Y) = 0.02 m, channel inlet velocity (V) = 0.677 m/s, and slot aperture size (x) = 0.15 m	325
Fig. 8.34	Numerically simulated velocity distribution inside rectangular SIT with depth of flow (Y) = 0.02 m, channel inlet velocity (V) = 0.677 m/s, and slot aperture size (x) = 0.03 m	326
Fig. 8.35	Numerically simulated velocity distribution inside irregular hexagonal SIT with depth of flow (Y) = 0.02 m, channel inlet velocity (V) = 0.677 m/s, and slot aperture size (x) = 0.15 m	327
Fig. 8.36	Numerically simulated velocity distribution inside irregular hexagonal SIT with depth of flow (Y) = 0.02 m, channel inlet velocity (V) = 0.677 m/s, and slot aperture size (x) = 0.03 m	328

Fig. 8.37	Numerically simulated velocity distribution inside trapezoidal SIT with depth of flow (Y) = 0.02 m, channel inlet velocity (V) = 0.677 m/s, and slot aperture size (x) = 0.15 m	329
Fig. 8.38	Numerically simulated velocity distribution inside trapezoidal SIT with depth of flow (Y) = 0.02 m, channel inlet velocity (V) = 0.677 m/s, and slot aperture size (x) = 0.03 m	330
Fig. 8.39	2D simulated velocity vector field in: (a) Depth of SIT y = 0.23 m (b) Depth of SIT y = 0.28 m (c) Depth of SIT y = 0.33 m (d) Depth of SIT y = 0.38 m (e) Depth of SIT y = 0.43 m (f) Depth of SIT y = 0.48 m (g) Depth of SIT y = 0.53 m (h) Depth of SIT y = 0.58 m (i) Depth of SIT y = 0.65 m (j) Depth of SIT y = 0.70 m ; at slot aperture size (x) = 0.15 m; depth of flow (Y) = 0.02 m and channel inlet velocity (V) = 0.677 m/s in rectangular SIT	331 to 335
Fig. 8.40	2D simulated velocity vector field in: (a) Depth of SIT y = 0.23 m (b) Depth of SIT y = 0.28 m (c) Depth of SIT y = 0.33 m (d) Depth of SIT y = 0.38 m (e) Depth of SIT y = 0.43 m (f) Depth of SIT y = 0.48 m (g) Depth of SIT y = 0.53 m (h) Depth of SIT y = 0.58 m (i) Depth of SIT y = 0.65 m (j) Depth of SIT y = 0.70 m ; at slot aperture size (x) = 0.15 m; depth of flow (Y) = 0.02 m and channel inlet velocity (V) = 0.677 m/s in irregular hexagonal SIT	336 to 340
Fig. 8.41	2D simulated velocity vector field in: (a) Depth of SIT y = 0.23 m (b) Depth of SIT y = 0.28 m (c) Depth of SIT y = 0.33 m (d) Depth of SIT y = 0.38 m (e) Depth of SIT y = 0.43 m (f) Depth of SIT y = 0.48 m (g) Depth of SIT y = 0.53 m (h) Depth of SIT y = 0.58 m (i) Depth of SIT y = 0.65 m (j) Depth of SIT y = 0.70 m ; at slot aperture size (x) = 0.15 m; depth of flow (Y) = 0.02 m and channel inlet velocity (V) = 0.677 m/s in trapezoidal SIT	341 to 345
Fig. 8.42	3D simulated velocity vector field at flow depth (Y) = 0.02 m and slot aperture size (x) = 0.15 m in rectangular SIT of depths: (a) y = 0.23 m (b) y = 0.28 m (c) y = 0.33 m (d) y = 0.38 m (e) y = 0.43 m (f) y = 0.48 m (g) y = 0.53 m (h) y = 0.58 m (i) y = 0.65 m (j) y = 0.70 m	346 to 347
Fig. 8.43	3D simulated velocity vector field in rectangular SIT of depth (y) = 0.23 m with slot aperture size (x) = 0.15 m, at flow depths: (a) Y = 0.04 m (b) Y = 0.06 m	348
Fig. 8.44	3D simulated velocity vector field at flow depth (Y) = 0.02 m and slot aperture size (x) = 0.15 m in irregular hexagonal SIT of depths: (a) y = 0.23 m (b) y = 0.28 m (c) y = 0.33 m (d) y = 0.38 m (e) y = 0.43 m (f) y = 0.48 m (g) y = 0.53 m (h) y = 0.58 m (i) y = 0.65 m (j) y = 0.70 m	349 to 350
Fig. 8.45	3D simulated velocity vector field in irregular hexagonal SIT of depth (y) = 0.23 m with slot aperture size (x) = 0.15 m, at flow depths: (a) Y = 0.04 m (b) Y = 0.06 m	351

Fig. 8.46	3D simulated velocity vector field at flow depth (Y) = 0.02 m and slot aperture size (x) = 0.15 m in trapezoidal SIT of depths: (a) y = 0.23 m (b) y = 0.28 m (c) y = 0.33 m (d) y = 0.38 m (e) y = 0.43 m (f) y = 0.48 m (g) y = 0.53 m (h) y = 0.58 m (i) y = 0.65 m (j) y = 0.70 m	352 353
Fig. 8.47	3D simulated velocity vector field in trapezoidal SIT of depth (y) = 0.23 m with slot aperture size (x) = 0.15 m, at flow depths: (a) Y = 0.04 m (b) Y = 0.06 m	354
Fig. 8.48	3D simulated colour-filled velocity contours at flow depth (Y) = 0.02 m and slot aperture size (x) = 0.15 m in rectangular SIT of depths: (a) y = 0.23 m (b) y = 0.28 m (c) y = 0.33 m (d) y = 0.38 m [flow is from left to right]	355
Fig. 8.49	3D simulated colour-filled velocity contours in rectangular SIT of depth (y) = 0.23 m with slot aperture size (x) = 0.15 m at flow depths: (a) Y = 0.04 m (b) Y = 0.06 m [flow is from left to right]	356
Fig. 8.50	3D simulated colour-filled velocity contours at flow depth (Y) = 0.02 m and slot aperture size (x) = 0.15 m in irregular hexagonal SIT of depths: (a) y = 0.23 m (b) y = 0.28 m (c) y = 0.33 m (d) y = 0.38 m [flow is from left to right]	357
Fig. 8.51	3D simulated colour-filled velocity contours in irregular hexagonal SIT of depth (y) = 0.23 m with slot aperture size (x) = 0.15 m at flow depths: (a) Y = 0.04 m (b) Y = 0.06 m [flow is from left to right]	358
Fig. 8.52	3D simulated colour-filled velocity contours at flow depth (Y) = 0.02 m and slot aperture size (x) = 0.15 m in trapezoidal SIT of depths: (a) y = 0.23 m (b) y = 0.28 m (c) y = 0.33 m (d) y = 0.38 m [flow is from left to right]	359
Fig. 8.53	3D simulated colour-filled velocity contours in trapezoidal SIT of depth (y) = 0.23 m with slot aperture size (x) = 0.15 m at flow depths: (a) Y = 0.04 m (b) Y = 0.06 m [flow is from left to right]	360
Fig. 8.54a	3D and 2D simulated and experimentally observed water surface profiles with slot aperture size (x) = 0.15 m at depths of flow (Y) = 0.02, 0.04, and 0.06 m, in rectangular SIT of depth (y) = 0.23 m	362
Fig. 8.54b	3D and 2D simulated and experimentally observed water surface profiles with slot aperture size (x) = 0.03 m at depths of flow (Y) = 0.02, 0.04, and 0.06 m, in rectangular SIT of depth (y) = 0.23 m	363
Fig. 8.55a	3D and 2D simulated and experimentally observed water surface profiles with slot aperture size (x) = 0.15 m at depths of flow (Y) = 0.02, 0.04, and 0.06 m, in irregular hexagonal SIT of depth (y) = 0.23 m	364
Fig. 8.55b	3D and 2D simulated and experimentally observed water surface profiles with slot aperture size (x) = 0.03 m at depths of flow (Y) = 0.02, 0.04, and 0.06 m, in irregular hexagonal SIT of depth (y) = 0.23 m	365

Fig. 8.56a	3D and 2D simulated and experimentally observed water surface profiles with slot aperture size (x) = 0.15 m at depths of flow (Y) = 0.02, 0.04, and 0.06 m, in trapezoidal SIT of depth (y) = 0.23 m	366
Fig. 8.56b	3D and 2D simulated and experimentally observed water surface profiles with slot aperture size (x) = 0.03 m at depths of flow (Y) = 0.02, 0.04, and 0.06 m, in trapezoidal SIT of depth (y) = 0.23 m	367
Fig. 8.57	Vertical streamwise velocity profiles along the flow depth (Y or h) at the centre of the flume at a distance of 2.5 m from the flume's inlet, measured by 2D-PIV, predicted by 3D-CFD simulations and Yang <i>et al.</i> 2004 Eq. (4.3) at flow depths: (a) Y or h = 0.02 m (b) Y or h = 0.04 m (c) Y or h = 0.06 m	368
Fig. 8.58	Effect of single-pass and multi-pass cross correlation methods on velocity vector field and pattern of flow structures with respect to depth of SIT (y) in rectangular SIT with slot size (x) = 0.15 m at: (a) Y = 0.02 m, y = 0.28 m (b) Y = 0.02 m, y = 0.33 m; with CFD validation	379
Fig. 8.59	Effect of single-pass and multi-pass cross correlation methods on velocity vector field and pattern of flow structures with respect to flow depth (Y) in rectangular SIT with slot size (x) = 0.15 m at: (a) Y = 0.02 m, y = 0.28 m (b) Y = 0.04 m, y = 0.28 m; with CFD validation	380
Fig. 9.1	Spreadsheet showing experimental input data processed according to non-dimensional independent variables alongwith the measured and predicted particle trap efficiency of rectangular SIT, prior to the start of the regression analysis (total data points=96)	402
Fig. 9.2	SOLVER function dialogue box as a link between the SOLVER function and the data in the spreadsheet	403
Fig. 9.3	SOLVER function options for all iterative methods	404
Fig. 9.4	SOLVER function options for GRG iterative method	405
Fig. 9.5	Spreadsheet showing the solution of the selected empirical regression model (predicted particle trap efficiency of rectangular SIT) after the regression analysis (total data points = 96)	407
Fig. 9.6	Observed and regression model-predicted particle trap efficiency of rectangular SIT: (a) model development data set (b) validation data set (c) error range of model development data set (d) comparison with 3D-CFD predictions	411
Fig. 9.7	Observed and regression model-predicted particle trap efficiency of irregular hexagonal SIT: (a) model development data set (b) validation data set (c) error range of model development data set (d) comparison with 3D CFD predictions	412
Fig. 9.8	Observed and regression model-predicted particle trap efficiency of trapezoidal SIT: (a) model development data set (b) validation data set	413

(c) error range of model development data set (d) comparison with 3D
CFD predictions

LIST OF TABLES

Table 4.1	Dimensions and parametric details of physical model used in PIV study	136
Table 4.2a	Average velocity in open channel flume	148
Table 4.2b	Average streamwise velocities along the flow depth at the centre of an open channel flume at a distance of 2.5 m from the flume's inlet	149
Table 4.3	Average velocity on the streamwise central 2D vertical plane inside rectangular, irregular hexagonal and trapezoidal SITs measured by 2D-PIV	155
Table 4.4	Averaged velocities along flow depth at the centre of an open channel flume at a distance of 2.5 m from the flume's inlet measured by 2D-PIV with single-pass and multi-pass cross correlation method	157
Table 5.1	Physical model parameters used in the present study	168
Table 5.2	Flow parameters used in the present study	168
Table 5.3	Sediment parameters used in the present study	169
Table 5.4	Details of geometry used in the numerical modeling corresponding to flow depths	174
Table 5.5	Numerical model settings, operating conditions, solution methods and solution initialization details	180
Table 5.6	Trap efficiency results for different sewage solid particle size ranges	182
Table 5.7	Trap efficiency results for sewage solid particle size range R_1 and R_2 with two extra lid thicknesses	191
Table 6.1	Sediment invert trap (SIT) and open channel parameters	203
Table 6.2	Sedimentation parameter range (Raudkivi 1990)	216
Table 6.3	Sediment parameters	226
Table 6.4	Flow parameters	226
Table 8.1	Experimental and 2D CFD observations of particle trap efficiency of rectangular SIT with sewer solid size range SS_1SR_1	261
Table 8.2	Experimental and 3D CFD observations of particle trap efficiency of rectangular SIT with sewer solid size range SS_1SR_1	262
Table 8.3	Experimental and simulated (2D and 3D) observations of particle trap efficiency of rectangular SIT with sewer sediment size range SS_1SR_3	263
Table 8.4	Experimental and simulated (2D and 3D) observations of particle trap efficiency of rectangular SIT with sewer sediment size range SS_2SR_1	264
Table 8.5	Experimental and simulated (2D and 3D) observations of particle trap efficiency of rectangular SIT with sewer sediment size range SS_2SR_2	265
Table 8.6	Experimental and simulated (2D and 3D) observations of particle trap efficiency of irregular hexagonal SIT with sewer sediment size range SS_1SR_1	266

Table 8.7	Experimental and simulated (2D and 3D) observations of particle trap efficiency of irregular hexagonal SIT with sewer sediment size range SS_1SR_2	267
Table 8.8	Experimental and simulated (2D and 3D) observations of particle trap efficiency of irregular hexagonal SIT with sewer sediment size range SS_1SR_3	268
Table 8.9	Experimental and simulated (2D and 3D) observations of particle trap efficiency of irregular hexagonal SIT with sewer sediment size range SS_2SR_1	269
Table 8.10	Experimental and simulated (2D and 3D) observations of particle trap efficiency of irregular hexagonal SIT with sewer sediment size range SS_2SR_2	270
Table 8.11	Experimental and simulated (2D and 3D) observations of particle trap efficiency of trapezoidal SIT with sewer sediment size range SS_1SR_1	271
Table 8.12	Experimental and simulated (2D and 3D) observations of particle trap efficiency of trapezoidal SIT with sewer sediment size range SS_1SR_2	272
Table 8.13	Experimental and simulated (2D and 3D) observations of particle trap efficiency of trapezoidal SIT with sewer sediment size range SS_1SR_3	273
Table 8.14	Experimental and simulated (2D and 3D) observations of particle trap efficiency of trapezoidal SIT with sewer sediment size range SS_2SR_1	274
Table 8.15	Experimental and simulated (2D and 3D) observations of particle trap efficiency of trapezoidal SIT with sewer sediment size range SS_2SR_2	275
Table 8.16a	Average streamwise velocities along the flow depth at the centre of an open channel flume at a distance of 2.5 m from the flume's inlet	370
Table 8.16b	Average velocity across the cross section in an open channel flume	370
Table 8.17	Average velocity on the 2D vertical plane in rectangular SIT	374
Table 8.18	Average velocity on the 2D vertical plane in irregular hexagonal SIT	375
Table 8.19	Average velocity on the 2D vertical plane in trapezoidal SIT	375
Table 8.20	Average velocities along flow depth at the centre of an open channel flume at a distance of 2.5 m from the flume's inlet measured by 2D-PIV with single-pass and multi-pass cross correlation method	378
Table 9.1	Experimental data range	387
Table 9.2	Range of non-dimensional independent variables of the present study used for model development	387
Table 9.3	Experimental data set for rectangular, irregular hexagonal and trapezoidal SITs	398
Table 9.4	Sensitivity analysis of $\eta_{\text{rectangular SIT}}$ with 10% increase and decrease in dimensionless independent input variables	414
Table 9.5	Sensitivity analysis of $\eta_{\text{irregular hexagonal SIT}}$ with 10% increase and decrease in dimensionless independent input variables	414
Table 9.6	Sensitivity analysis of $\eta_{\text{trapezoidal SIT}}$ with 10% increase and decrease in dimensionless independent input variables	415

LIST OF SYMBOLS

S_p	Sedimentation parameter
C_a	Capillary number
k or k_p	Turbulence kinetic energy
k	Von-Karman constant
y_f	Vertical distance from channel bed to the free water surface
y_o	Vertical distance where velocity is hypothetically zero
y	Depth of sediment invert trap (SIT)
l	Length of sediment invert trap (SIT)
b	Width of an sediment invert trap (SIT)
x	Slot aperture size
t	Thickness of upstream and downstream lids
L	Characteristic length, Length of the flume
B	Width of the flume or open channel
Y or h	Depth of flow in open channel
H	Depth of the flume
S_{α_b}	Source term
S, S_o	Open channel bed slope or gradient
Q	Discharge/Flow rate
A	Wetted area
P	Wetted perimeter of open channel
P	Pressure
P	Porosity
V_p	Volume of pores or voids
V	Total volume of the mixture
R_h	Hydraulic radius
D	Hydraulic diameter
u_*, V_*	Bed shear velocity
F_r	Froude number
r_m	Mean ratio of longest to the shortest diameters
R_h	Hydraulic radius of open channel
Re	Fluid Reynold number
Re	Particle relative Reynolds number
R_{*c}	Critical shear Reynold number
D_p	Diameter of sewage solid particles used in present study
G	Specific gravity of sewer sediment particles
w_s	Fall velocity of particles
A_p	Average projected area of randomly oriented particles

m_{ba} and m_{ab}	Transition of mass transfer between phases
m_p	Mass of the particle
U_{*c}	Critical bed shear velocity
\vec{u}_b	Average velocity of secondary phase: water
\vec{u}_p	Average velocity of particle
V	Mean or average velocity of the fluid measured by EMF
V_a	Mean or average flow velocity in the open channel
U_p	Velocity of the particle falling in the moving fluid.
U_{px} and U_{py}	Horizontal and vertical components of particle fall velocity in the moving fluid, respectively
\vec{u}, \bar{U}	Velocity of the fluid phase
u or $u_{x,y,z,t}$	Flow velocity at a point in x-direction
v or $v_{x,y,z,t}$	Flow velocity at a point in y-direction
w or $w_{x,y,z,t}$	Flow velocity at a point in z-direction
\bar{u} or $\overline{u_{x,y,z}}$	Average of flow velocity at a point in x-direction
\bar{v} or $\overline{v_{x,y,z}}$	Average of flow velocity at a point in y-direction
\bar{w} or $\overline{w_{x,y,z}}$	Average of flow velocity at a point in z-direction
u' or $u'_{x,y,z,t}$	Fluctuating component of mean flow velocity at a point in x-direction
v' or $v'_{x,y,z,t}$	Fluctuating component of mean flow velocity at a point in y-direction
w' or $w'_{x,y,z,t}$	Fluctuating component of mean flow velocity at a point in z-direction
u_{rms}	Standard deviation of the turbulent velocity fluctuations u'
v_{rms}	Standard deviation of the turbulent velocity fluctuations v'
w_{rms}	Standard deviation of the turbulent velocity fluctuations w'
$d_{84.1}$	Sediment size for which 84.1 percent of the material by weight is finer
d_{50}	Sediment size for which 50 percent of the material by weight is finer
$d_{15.9}$	Sediment size for which 15.9 percent of the material by weight is finer
d_g	Geometric mean diameter
\vec{F}	Additional acceleration (force per unit mass of particle), external forces
C_D	Drag coefficient
F_D	Drag force
F_{PG}	Pressure gradient force
F_{VM}	Virtual mass force
F_L	Saffman lift force
g	Acceleration due to gravity
c	Constant
d	Particle diameter, mean sediment diameter
d_n	Nominal or equivalent diameter
d_p	Average equivalent spherical diameter
d_{sieve}	Sieve diameter

a_1, a_2, a_3	Constants based on Reynolds number R_e
$R_{e_{sph}}$	Reynolds number based on equivalent spherical diameter of particle
d_{sph}	Equivalent spherical diameter (m)
SA_{sphere}	Surface area of a sphere with equal volume as that of particle
$SA_{particle}$	Surface area of real particle
u_t, U_t	Terminal fall velocity of particle in fluid
b_1	$e^{(2.3288-6.4581\phi+2.4486\phi^2)}$
b_2	$0.0964 + 0.5565\phi$
b_3	$e^{(4.905-13.8944\phi+18.4222\phi^2-102599\phi^3)}$
b_4	$e^{(1.4681+12.2584\phi-20.7322\phi^2+15.8855\phi^3)}$
V_x, V_y, V_z	Velocity of fluid in x , y and z -directions
W	Specific weight of sediment at the end of T years
W_e	Webber number
Y	Depth of flow in open channel
y_v	Thickness of physical viscous sublayer
m_p	Particle mass

Greek symbols

α_a	Proportion of volume of primary phase: air
α_b	Proportion of volume of secondary phase: water
ρ_p	Density of sewer sediment particles used in present study
ρ_a	Density of primary phase: air
ρ_b	Density of secondary phase: water
ρ_r	Relative density of the particle in water
ρ_s	Dry density of the sediment
τ_{*c}	Non-dimensional critical shear stress
τ_c	Critical shear stress
τ_o or τ_b	Normal bed shear stress
τ_r	Time of particle relaxation
μ	Molecular or dynamic viscosity of fluid
μ_t	Eddy viscosity
ρ, ρ_f	Density of fluid
ϵ	Rate of dissipation of turbulence energy
ϕ	Particle shape factor
η	Particle trap efficiency of an irregular hexagonal invert trap
γ_s	Specific weight of the sediment particle
γ_s	Specific weight of the fluid
σ	Standard deviation
σ	Surface tension
σ_g	Geometric standard deviation

Ψ	Angle of repose
ν	Kinematic viscosity of the fluid
δ_s	Laminar sub-layer
δt	Duration of each laser pulse
Δt	Camera exposure
Π	Wake strength parameter of Cole

LIST OF ABBREVIATIONS

ADCP	Acoustic Doppler Current Profiler
ADV	Acoustic Doppler Velocimetry
AGU	American Geophysical Union
ANN	Artificial Neural Network
AS	Absolute Sensitivity
ASCE	American Society of Civil Engineers
ASM	Algebraic Stress Model
BGM	Bounded Gradient Maximization
BSS	Bed Shear Stress
CIRIA	Construction Industry Research and Information Association
CSS	Combined Sewer System
CFD	Computational Fluid Dynamics
CPHEEO	Central Public Health and Environment Engineering Organization
CSDT	Combined Sewage Detention Tank
CSO	Combined Sewer Overflow
DPM	Discrete Phase Model
EMF	Electro Magnetic Flowmeter
FG	Flush Gate
FLM	Fixed Lid Model
GCI	Grid Convergence Index
GGCB	Green-Gauss Cell-Based
GGNB	Green-Gauss Node-Based
GPT	Gross Pollutant Trap
GRG	Generalized Reduced Gradient
HDVS	Hydrodynamic Vortex Separator
HP	Horse Power
HRIC	High Resolution Interface Capturing
LBM	Lattice Boltzman Method
LDV	Laser Doppler Velocimetry
LSCB	Least Squares Cell-Based
MAPE	Mean Absolute Percentage Error
MUSCL	Monotone Upstream Centered Schemes for Conservation Laws

NBS	Near Bed Solids
N-S	Navier-Stokes
ODE	Ordinary Differential Equation
PC	Personal Computer
PISO	Pressure-Implicit with Splitting of Operators
PIV	Particle Image Velocimetry
POW	Power Law Scheme
PRESTO	PREssure STaggering Option
PSD	Particle Size Distribution
RANS	Reynolds Averaged Navier-Stokes
RE	Relative Error
RMSE	Root Mean Square Error
RS	Relative Sensitivity
SCPT	System for Catchment, Pre-treatment and Treatment
SEM	Scanning Electron Microscope
SIMPLE	Semi-Implicit Method for Pressure-Linked Equations
SIMPLEC	Semi-Implicit Method for Pressure Linked Equations-Consistent
SIT	Sediment Invert Trap
SSIIM	Sediment Simulation in Intakes with Multiblock Options
SOU	Second Order Upwind Scheme
SST	Shear Stress Transport
TKE	Turbulent Kinetic Energy
TSS	Total Suspended Solids
NBS	Near bed solids
VOF	Volume of Fluid
WWTP	Waste Water Treatment Plant
2D	Two-Dimensional
3D	Three-Dimensional
u/s	Upstream
d/s	Downstream
vs	Versus